BMC Medical Imaging

RESEARCH

Open Access

Using apparent diffusion coefficient maps and radiomics to predict pathological grade in upper urinary tract urothelial carcinoma

Rile Nai[1], Kexin Wang[2], Shuai Ma[1], Zuqiang Xi[3], Yaofeng Zhang[3], Xiaodong Zhang[1] and Xiaoying Wang[1*]

Abstract

Background The apparent diffusion coefficient (ADC) has been reported as a quantitative biomarker for assessing the aggressiveness of upper urinary tract urothelial carcinoma (UTUC), but it has typically been used only with mean ADC values. This study aims to develop a radiomics model using ADC maps to differentiate UTUC grades by incorporating texture features and to compare its performance with that of mean ADC values.

Methods A total of 215 patients with histopathologically confirmed UTUC were enrolled retrospectively and divided into training and test sets. The optimum cutoff value for the mean ADC was derived using the receiver operating characteristic (ROC) curve. Radiomics features based on ADC maps were extracted and screened, and then a radiomics model was constructed. Both mean ADC values and the radiomics model were tested on the training and test sets. ROC curve and DeLong test were used to assess the diagnostic performance.

Results The training set consisted of 151 patients (median age: 68.0, IQR: [63.0, 75.0] years; 80 males), whereas the test set consisted of 64 patients (median age: 68.0, IQR: [61.0, 72.3] years; 31 males). The ADC values were significantly lower in high-grade versus low-grade UTUC (1310×10^{-6}mm^2/s vs. 1480×10^{-6}mm^2/s, $p<0.001$). The area under the curve (AUC) values of the mean ADC values in the training and test sets were 0.698 [95% confidence interval [CI]: 0.625–0.772] and 0.628 [95% CI: 0.474–0.782], respectively. Compared with the mean ADC values, the ADC-based radiomics model, which incorporates features such as log-sigma-1-0-mm-3D_glcm_ClusterProminence and wavelet-LLL_firstorder_10Percentile, obtained a significantly greater AUC in the training set (AUC: 1.000, 95% CI: 1.000–1.000, $p<0.001$), and a trend towards statistical significance in the test set (AUC: 0.786, 95% CI: 0.651–0.921, $p=0.071$).

Conclusions The ADC-based radiomics model showed promising potential in predicting the pathological grade of UTUC, outperforming the mean ADC values in classification accuracy. Further studies with larger sample sizes and external validation are necessary to confirm its clinical utility and generalizability.

Clinical trial number Not applicable.

Keywords Upper urinary tract urothelial carcinoma, Pathological grade, Apparent diffusion coefficient, Radiomics

*Correspondence:
Xiaoying Wang
wangxiaoying@bjmu.edu.cn
[1]Department of Radiology, Peking University First Hospital, 8, Xishiku Street, Xicheng District, Beijing 100034, China
[2]School of Basic Medical Sciences, Capital Medical University, 10, Xitoutiao, Youanmenwai, Fengtai District, Beijing 100069, China
[3]Beijing Smart Tree Medical Technology Co., Ltd., 24, Huangsi Avenue, Xicheng District, Beijing 100035, China

Introduction

Upper urinary tract urothelial carcinoma (UTUC) is a relatively uncommon malignancy originating in the renal pelvis and ureter, accounting for approximately 5–10% of all urothelial carcinoma cases [1]. Histologically, UTUC can be classified into low-grade and high-grade cancers, with different grades exhibiting varying levels of aggressiveness [2]. The pathological grade is crucial for guiding management decisions and serves as an independent predictor of mortality in UTUC patients [3, 4].

Ureteroscopy combined with ureteroscopic biopsy aids in diagnosing UTUC; however, challenges in specimen collection and biopsy limitations hinder the accuracy of determining the pathological grade and tumor stage [5, 6]. Moreover, ureteroscopy and biopsy pose a risk for intravesical recurrence [7]. Consequently, a non-invasive evaluation method is essential for preoperatively predicting the grade of UTUC tumors.

Recently, magnetic resonance imaging (MRI) has been widely used as a non-invasive preoperative risk assessment method for malignant tumors utilizing functional and molecular imaging technology [8, 9]. Diffusion-weighted imaging (DWI) within MRI can identify the histological type of malignant tumors by the diffusion of water molecules, quantified by the apparent diffusion coefficient (ADC) value [10, 11]. Multi-b value DWI has shown promise in improving the staging and assessment of biological aggressiveness in urogenital cancers [12, 13]. Some studies suggest that the mean ADC value may serve as a quantitative biomarker reflecting the aggressiveness of UTUC [14–16]. However, these studies have several limitations, such as small sample sizes and the reliance on traditional partial-lesion single-slice ADC measurements. Additionally, the overlap of ADC values between low- and high-grade tumors complicates the accurate grading of UTUC based solely on ADC values [17]. Therefore, distinctive imaging features that accurately capture diffusion patterns and tissue heterogeneity are crucial for reliable UTUC grading.

In contrast to the mean ADC values, radiomics extracts more quantitative features from ADC maps by using data-characterization algorithms [18, 19]. Recently, radiomics has been reported to achieve greater precision in the diagnosis, grading, staging and prognosis of many tumors on ADC maps, especially those of bladder cancer [20, 21]. However, to date, no radiomics models based on MRI, specifically ADC maps, have been developed for differentiating between low- and high-grade UTUC. This gap in the existing literature underscores the unique contribution of our study. Therefore, the aim of this study was to develop an ADC-based radiomics model and to assess its classification performance in comparison to mean ADC values.

Materials and methods

This retrospective study was approved by the institutional ethics review board, which waived the requirement for informed consent (IRB number: 2023437).

Patients

A total of 254 consecutive patients with pathologically confirmed UTUC who underwent multiparametric MRI examinations between January 2010 and December 2023 were enrolled in our study. The inclusion criteria for patients were as follows: (1) were diagnosed with UTUC through pathological examination following radical nephroureterectomy; and (2) had MRI images collected within 3 months before the surgical procedure, with DWI scans with low (b=0 s/mm^2) and high (b=800, 1000, or 1200 s/mm^2) b values. The exclusion criteria were as follows: (1) had a history of any treatment, including chemotherapy or radiotherapy, before MRI; (2) had severe artifacts that could make segmentation of cancer difficult on MR images; and (3) had incomplete clinical data. Finally, 215 patients were found to be eligible for this study and were divided into low- and high-grade groups according to their pathological results (low-grade, 39 patients; high-grade, 176 patients). Figure 1 shows the flow diagram of patient recruitment. The clinical baseline characteristics collected included the patient's age, sex, hydronephrosis status, tumor location, and tumor type.

MRI sequences

All the data used in our study were anonymized. All the images were acquired as axial DW images of patients in the supine position. These images were obtained using different b values on MR scanners from eight different vendors at our institution utilizing a phased-array coil. ADC maps were generated after DWI data acquisition using software from each scanner. The detailed imaging parameters for each scanner are provided in Table 1.

Image delineation

A radiologist with 5 years of experience in body MR imaging manually delineated the entire tumor of a UTUC on axial images of the ADC layer by layer using ITK-SNAP 3.6.0 (http://www.itk-snap.org/) to obtain the vol ume of interest (VOI) for the corresponding area of the UTUC tumor. T2-weighted imaging (T2WI) was used to determine the edges of the lesion. Each segmented lesion was further refined under the guidance of a senior radiologist with more than 15 years of experience in body MR imaging to ensure precise tumor margins. In cases of disagreement, the results were reached through discussion. The volume, size and mean ADC value were extracted from the VOI for separate analysis. One month later, the VOI of UTUC tumors of 30 randomly selected patients was re-segmented by the radiologist to evaluate

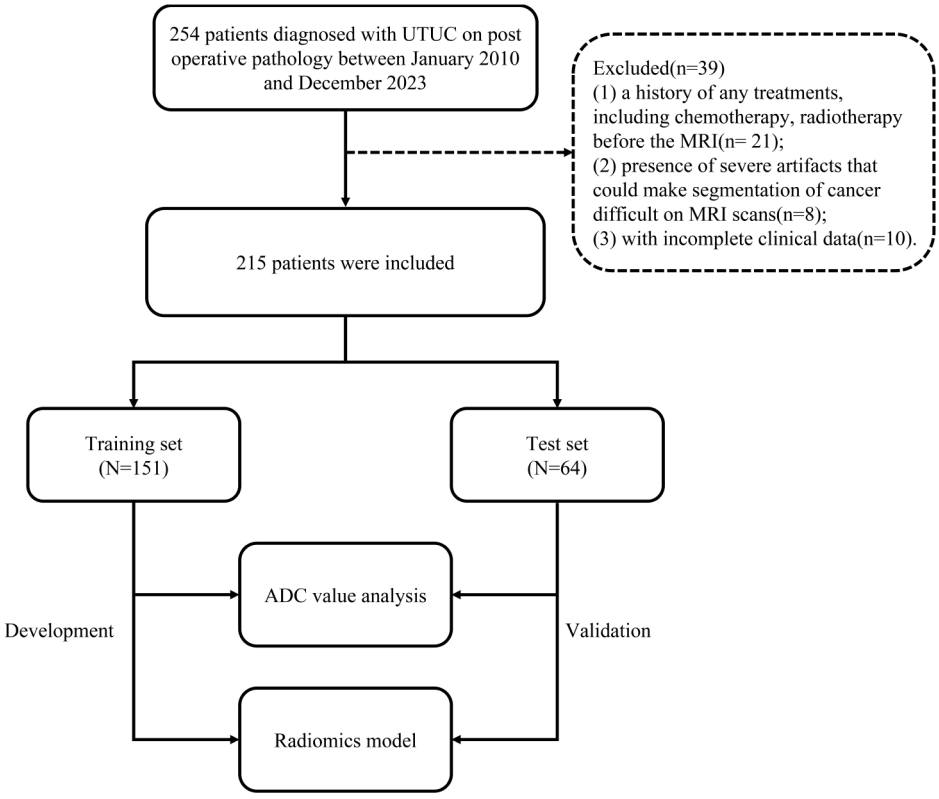

Fig. 1 The flowchart of patient selection

the inter-class correlation coefficient (ICC) of the delineated image features within observers.

ADC value analysis

The optimal cutoff value for the mean ADC for grading UTUC was determined using the receiver operating characteristic (ROC) curve method on the training set, using pathology reports post-excision as the gold standard. This cutoff value was validated in the test set.

Radiomics modeling

The modeling workflow included the following steps: (a) feature extraction, (b) model construction, and (c) predictive performance validation. Radiomics features were extracted using the PyRadiomics package in Python. A total of 1070 features were extracted from the ADC map of each tumor. More information about radiomic model construction is provided in Supplemental Material, Table S2. The average performance metrics of the trained models were evaluated by 5-fold cross validation in the training set, and the best model was then selected. The test set was used to evaluate the predictive effect of the radiomics model for grading UTUC. All processes of constructing and validating the radiomics models were implemented in Python (v 3.6.0). An overview of the radiomics model development and the diagnostic performance evaluation process is shown in Fig. 2.

Diagnostic performance evaluation

The ROC curves were used to evaluate the classification performance of the mean ADC values and the radiomics model in both the training and test sets. The area under the curve (AUC) with the 95% confidence interval (CI), sensitivity, and specificity were calculated. The DeLong test was used to compare the AUC of the mean ADC value and the radiomics model, and $P<0.05$ was considered to indicate statistical significance.

Statistical analysis

Statistical analysis was performed using R version 4.1.3 (https://www.r-project.org/). The measurement data were tested for normality, and those that conformed to a normal distribution are expressed as the mean ± standard deviation. The independent samples t test was used for comparisons between two groups. Nonnormally distributed data are expressed as medians (upper and lower quartiles), and group comparisons were assessed using the Mann–Whitney U test. The enumeration data are expressed as the number of patients, and comparisons between two groups were performed with the χ^2 test.

Table 1 MR imaging parameters of diffusion-weighted imaging (DWI) sequences

	Achieva	Aera	DISCOVERY MR750	Ingenia	Multiva	Prisma	SIGNA EXCITE	uMR 790	Over all
	(*N* = 5)	(*N* = 31)	(*N* = 87)	(*N* = 22)	(*N* = 9)	(*N* = 3)	(*N* = 9)	(*N* = 49)	(*N* = 215)
Magnetic Field									
1.5T	0 (0%)	31 (100%)	0 (0%)	0 (0%)	9 (100%)	0 (0%)	4 (44.4%)	0 (0%)	44 (20.5%)
3.0T	5 (100%)	0 (0%)	87 (100%)	22 (100%)	0 (0%)	3 (100%)	5 (55.6%)	49 (100%)	171 (79.5%)
Repetition Time (ms)									
Median [Q1, Q3]	3000 [3000,3000]	4900 [4400,5600]	6920 [5580,8380]	1630 [1390,1680]	3000 [3000,3000]	4200 [4200,4200]	4330 [2300,4800]	3550 [3550,3550]	4400 [3550,6490]
Echo Time (ms)									
Median [Q1, Q3]	52.1 [52.1,52.7]	58.0 [58.0,58.0]	54.5 [53.7,54.8]	73.4 [71.8,74.8]	65.3 [65.0,65.3]	48.0 [47.0,48.0]	56.1 [56.0,69.4]	54.9 [54.9,56.9]	54.9 [54.5,58.0]
Pixel Band width (MHz)									
Median [Q1, Q3]	3710 [3640,3770]	1460 [1460,1460]	1950 [1950,1950]	2340 [2310,2340]	2700 [2700,2700]	2330 [2330,2330]	1950 [1950,1950]	2550 [2550,2550]	1950 [1950,2550]
B value (s/mm^2)									
Median [Q1, Q3]	800 [800,800]	800 [800,800]	1200 [1200,1200]	800 [800,800]	800 [800,800]	1000 [1000,1000]	800 [800,800]	1000 [1000,1000]	1000 [800,1200]
FOV (mm)									
Median [Q1, Q3]	375 [370,400]	400 [400,400]	360 [360,400]	350 [350,380]	375 [375,375]	380 [380,390]	380 [380,380]	399 [399,399]	399 [360,400]
Slice Thickness (mm)									
Median [Q1, Q3]	6.00 [5.00,6.00]	5.00 [5.00,5.00]	5.50 [5.00,6.00]	6.00 [6.00,6.00]	5.50 [5.00,6.00]	5.50 [5.25,5.75]	5.00 [5.00,5.00]	5.00 [5.00,5.00]	5.00 [5.00,6.00]
Slice Spacing (mm)									
Median [Q1, Q3]	7.00 [6.00,7.00]	6.00 [6.00,6.00]	6.00 [6.00,7.00]	7.00 [7.00,7.00]	6.50 [6.00,7.00]	6.60 [6.30,6.75]	6.00 [5.50,6.00]	6.00 [6.00,6.00]	6.00 [6.00,7.00]
Pixel Spacing (mm)									
Median [Q1, Q3]	1.93 [1.79,1.93]	2.33 [2.33,2.33]	1.41 [1.41,1.56]	1.22 [1.19,1.22]	1.95 [1.95,1.95]	1.42 [1.42,1.46]	1.48 [1.48,1.48]	0.780 [0.780,0.781]	1.41 [1.22,1.70]

Note UTUC, Upper urinary tract urothelial carcinoma. Q1, First quartile (25th percentile), Q3, Third quartile (75th percentile)

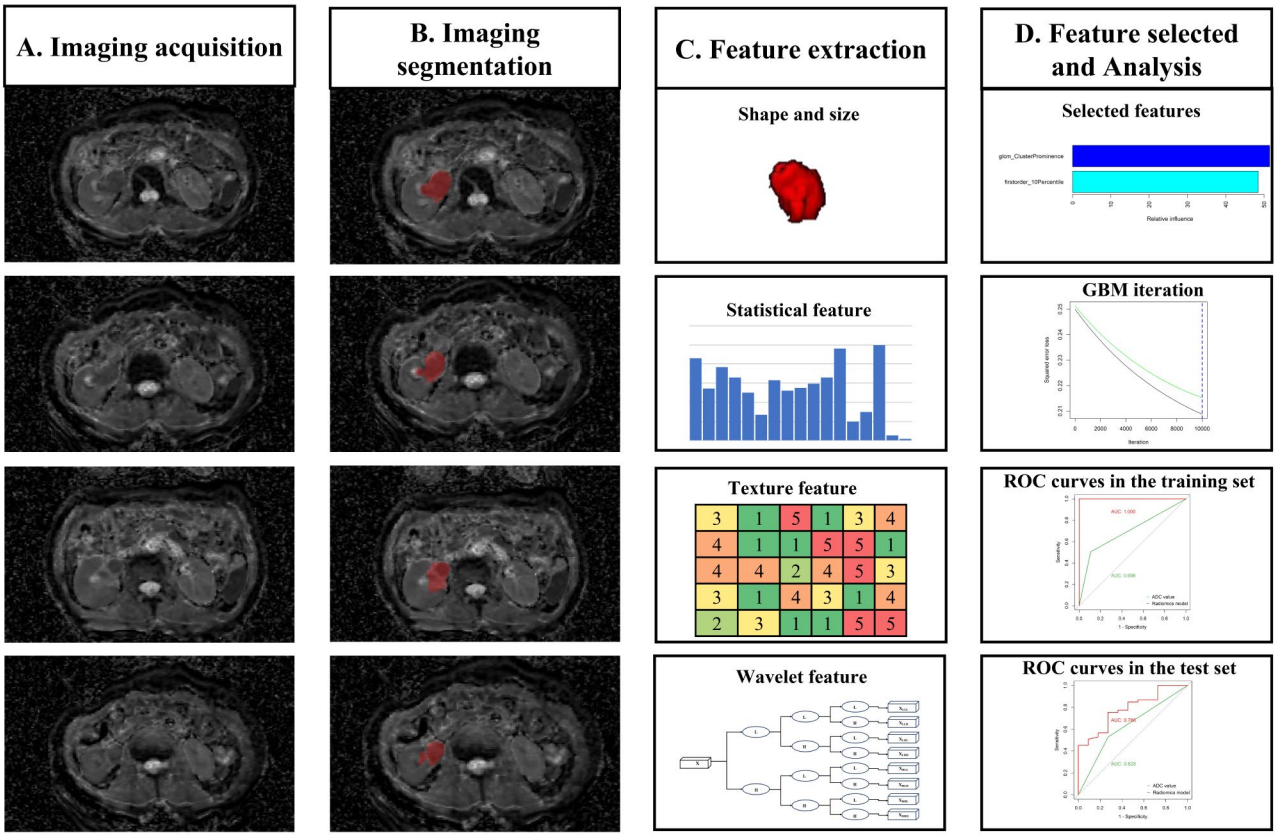

Fig. 2 The flowchart of the radiomics analysis. GBM, gradient boosting machine; ROC, operator characteristic curve

Results

Patient characteristics

In this study, a total of 215 patients who were diagnosed with UTUC were included and randomly assigned to the training set ($n=151$) or the test set ($n=64$) at a ratio of 7:3. Among the participants, there were 111 male patients and 104 female patients, with median ages of 68.0 years (interquartile range, 63.0–75.0 years) and 68.0 years (interquartile range, 61.0, 72.3), respectively. Table 2 shows the demographics and tumor grades of the patients in the two cohorts. High-grade UTUC accounted for 81.5% (123/151) and 82.8% (53/64) of the training and test sets, respectively, while low-grade UTUC accounted for 18.5% (28/151) and 17.2% (11/64) of the training and test sets, respectively. Notably, no statistically significant differences were observed in the clinical baseline characteristics between the training and test sets (all $p>0.05$). Furthermore, the mean ADC values were significantly lower in the high-grade group than in the low-grade group (1310 vs. 1480, $p<0.001$) (Table 3).

Feature selection and construction of feature datasets

The construction of the radiomics model is illustrated in Fig. 3. By calculating ICC ≥ 0.75, 951 features were preserved (see Table S1 in the supplementary material). To address the limited number of low-grade cases and dataset imbalance, upsampling was applied to balance the training set, followed by min–max normalization for standardization. Feature reduction using the Pearson correlation coefficient (threshold 0.99) reduced the feature set to 656, which was further refined to 2 features using Analysis of Variance (ANOVA). The key radiomic features identified were log-sigma-1-0-mm-3D_glcm_ClusterProminence and wavelet-LLL_firstorder_10Percentile, which formed the radiomics model. Gradient boosting classifiers were trained on these optimal features in the balanced training set. Figure 4 shows the distributions of the mean ADC values, UTUC grades, and Rad-score and UTUC grades in the training and test sets. Figure 5 shows comparative images of low-grade and high-grade lesions.

Evaluation of the mean ADC values and radiomics model performance

The comprehensive performance metrics of the mean ADC value and radiomics model, including the AUC (95% CI), accuracy, sensitivity, and specificity, are summarized in Table 4. The identified cutoff value for the ADC was $>1313\times10^{-6}$ mm^2/s (sensitivity=50.4%, specificity=89.3%) for distinguishing low-grade from

Table 2 Characteristics of the enrolled lesions in the training and test sets

	Overall	Training set	Test set	*P* value
	(*N* = 215)	(*N* = 151)	(*N* = 64)	
Grade classification				0.966
Low	39 (18.1%)	28 (18.5%)	11 (17.2%)	
High	176 (81.9%)	123 (81.5%)	53 (82.8%)	
Sex				0.645
Female	104 (48.4%)	71 (47.0%)	33 (51.6%)	
Male	111 (51.6%)	80 (53.0%)	31 (48.4%)	
Age (years)				0.538
Median [Q1, Q3]	68.0 [62.5, 74.0]	68.0 [63.0, 75.0]	68.0 [61.0, 72.3]	
Hematuria				0.783
No	66 (30.7%)	45 (29.8%)	21 (32.8%)	
Yes	149 (69.3%)	106 (70.2%)	43 (67.2%)	
Hydronephrosis				0.729
No	103 (47.9%)	74 (49.0%)	29 (45.3%)	
Yes	112 (52.1%)	77 (51.0%)	35 (54.7%)	
Smoking				0.218
No	172 (80.0%)	117 (77.5%)	55 (85.9%)	
Yes	43 (20.0%)	34 (22.5%)	9 (14.1%)	
History of UTUC				0.984
No	200 (93.0%)	141 (93.4%)	59 (92.2%)	
Yes	15 (7.0%)	10 (6.6%)	5 (7.8%)	
Tumor laterality				0.227
Left	106 (49.3%)	79 (52.3%)	27 (42.2%)	
Right	109 (50.7%)	72 (47.7%)	37 (57.8%)	
Tumor location				0.748
Renal pelvic	112 (52.1%)	81 (53.6%)	31 (48.4%)	
Ureter	89 (41.4%)	60 (39.7%)	29 (45.3%)	
Both	14 (6.5%)	10 (6.6%)	4 (6.3%)	
Multiple lesion				> 0.999
No	195 (90.7%)	137 (90.7%)	58 (90.6%)	
Yes	20 (9.3%)	14 (9.3%)	6 (9.4%)	
Tumor volume (mm^3)				0.669
Median [Q1, Q3]	5640 [2990, 13700]	5260 [2850, 14000]	6480 [3220, 13400]	
Tumor size				
X (mm)				0.741
Median [Q1, Q3]	22.5 [16.4, 35.8]	22.5 [16.4, 37.5]	22.4 [16.4, 31.4]	
Y (mm)				0.423
Median [Q1, Q3]	23.9 [16.9, 35.9]	23.6 [16.5, 35.8]	24.5 [19.6, 35.9]	
Z (mm)				0.309
Median [Q1, Q3]	36.0 [24.0, 48.0]	36.0 [22.3, 48.0]	38.0 [25.5, 48.3]	
ADC value ($\times 10^{-6} mm^2/s$)				0.495
Median [Q1, Q3]	1330 [1200, 1570]	1330 [1200, 1590]	1320 [1220, 1510]	

Note UTUC, Upper urinary tract urothelial carcinoma. ADC, Apparent diffusion coefficient. Q1, First quartile (25th percentile), Q3, Third quartile (75th percentile)

high-grade UTUC. In the training set, the AUC for the mean ADC was 0.698 (95% CI: 0.625–0.772), and in the test set, it was 0.628 (95% CI: 0.474–0.782). Conversely, the AUC values for the radiomics model were 1.000 (95% CI: 1.000–1.000) in the training set and 0.786 (95% CI: 0.651–0.921) in the test set. Comparative analysis revealed that the radiomics model outperformed the mean ADC value in assessing the preoperative UTUC grade in the training set ($P<0.001$). Although the performance of the radiomics model appeared superior to that of the mean ADC value in the test set, the difference did not reach statistical significance ($P=0.071$). In terms of sensitivity, the mean ADC value achieved 0.504 (95% CI: 0.416–0.592) in the training set and 0.528 (95% CI: 0.394–0.663) in the test set. In comparison, the radiomics model demonstrated superior sensitivity, reaching 1.000 (95% CI: 1.000–1.000) in the training set and 0.755 (95% CI: 0.639–0.871) in the test set. The ROC curves, illustrating the discriminatory abilities of both the mean ADC value and the radiomics model, are depicted in Fig. 6.

Discussion

In our study, we established an ADC-based radiomics model for grading UTUC preoperatively and noninvasively. We found that the radiomics model performed well in both the training (AUC = 1.000) and test (AUC = 0.786) sets. For the first time, we applied an ADC-based radiomics model to differentiate between low-grade and high-grade UTUC. Our findings can aid in the preoperative and noninvasive diagnosis of these two grades of tumors.

Both the European Association of Urology (EAU) and the American Urology Association (AUA) emphasize the significance of stratifying patients into low- or high-risk categories based on patient and tumor characteristics [2, 22]. Patients with low-risk disease may be offered kidney-sparing surgery (KSS) via ureteroscopy (URS), while patients with high-risk disease are indicated for radical surgery via radical nephroureterectomy (RNU). One of the factors that distinguishes high-risk patients from low-risk patients is the pathological grade of the tumor [2]. A diagnostic URS with a biopsy can yield information about tumor grade and the feasibility of endoscopic treatment, but this procedure costs time and resources, the sampling error of URS biopsy is well known [23], and there is a described increased risk of subsequent bladder recurrence after RNU among patients examined with a preoperative URS [24]. Therefore, the developed radiomics model may greatly benefit clinical decision-making by providing a noninvasive and quantitative method to differentiate between low- and high-grade UTUC.

The ADC is being increasingly adopted in clinical practice and is useful for differentiating benign from malignant abnormalities, assessing tumor aggressiveness, and

Table 3 Characteristics of the enrolled patients in the low- and high-grade groups

	Overall	Low-grade	High-grade	*P* value
	(*N* = 215)	(*N* = 39)	(*N* = 176)	
Dataset classification				0.966
Training set	151 (70.2%)	28 (71.8%)	123 (69.9%)	
Test set	64 (29.8%)	11 (28.2%)	53 (30.1%)	
Sex				> 0.999
Female	104 (48.4%)	19 (48.7%)	85 (48.3%)	
Male	111 (51.6%)	20 (51.3%)	91 (51.7%)	
Age (years)				0.845
Median [Q1, Q3]	68.0 [62.5, 74.0]	68.0 [62.5, 75.0]	68.0 [62.8, 74.0]	
Hematuria				0.558
No	66 (30.7%)	14 (35.9%)	52 (29.5%)	
Yes	149 (69.3%)	25 (64.1%)	124 (70.5%)	
Hydronephrosis				0.318
No	103 (47.9%)	22 (56.4%)	81 (46.0%)	
Yes	112 (52.1%)	17 (43.6%)	95(54.0%)	
Smoking				0.102
No	172 (80.0%)	27 (69.2%)	145 (82.4%)	
Yes	43 (20.0%)	12 (30.8%)	31 (17.6%)	
History of UTUC				0.216
No	200 (93.0%)	34 (87.2%)	166 (94.3%)	
Yes	15 (7.0%)	5 (12.8%)	10 (5.7%)	
Tumor laterality				0.797
Left	106 (49.3%)	18 (46.2%)	88 (50.0%)	
Right	109 (50.7%)	21 (53.8%)	88 (50.0%)	
Tumor location				0.433
Renal pelvic	112 (52.1%)	23 (59.0%)	89 (50.6%)	
Ureter	89 (41.4%)	15 (38.5%)	74 (42.0%)	
Both	14 (6.5%)	1 (2.6%)	13 (7.4%)	
Multiple lesion				0.195
No	195 (90.7%)	38 (97.4%)	157 (89.2%)	
Yes	20 (9.3%)	1 (2.6%)	19 (10.8%)	
Tumor volume (mm^3)				0.234
Median [Q1, Q3]	5640 [2990, 13700]	4350 [2950, 12300]	6140 [2990, 14200]	
Tumor size				
X (mm)				0480
Median [Q1, Q3]	22.5 [16.4, 35.8]	21.9 [17.8, 32.5]	23.3 [16.4, 37.2]	
Y (mm)				0.215
Median [Q1, Q3]	23.9 [16.9, 35.9]	21.9 [16.3, 34.2]	24.5 [17.1 35.9]	
Z (mm)				0.333
Median [Q1, Q3]	36.0 [24.0, 48.0]	35.0 [213.0, 44.5]	36.0 [24.0, 48.1]	
ADC value ($\times 10^{-6} mm^2/s$)				< 0.001
Median [Q1, Q3]	1330 [1200, 1570]	1480 [1330, 1730]	1310 [1190, 1540]	

Note UTUC, Upper urinary tract urothelial carcinoma. ADC, Apparent diffusion coefficient. Q1, First quartile (25th percentile), Q3, Third quartile (75th percentile)

evaluating tumor treatment [25–27]. Previous studies have suggested that evaluating ADC values might be useful for quantitatively characterizing the histopathology of UTUC [15, 16]. Our findings demonstrating significantly lower ADC values in high-grade UTUC than in low-grade UTUC, that are consistent with these prior results. However, ADC values only reflect the distribution of densities and cannot fully explore the potential value of imaging, such as shape features and the spatial heterogeneity of lesions. In our study, we mined high-throughput quantitative features from ADC maps, including intensity-based, structural, texture-based, and wavelet transform-based features. We then selected the most effective features and developed a radiomics model. Our findings demonstrated that the radiomics model exhibited notable performance in predicting the grade of UTUC, prominently featuring two key parameters: the first-order 10th percentile ADC value and gray level

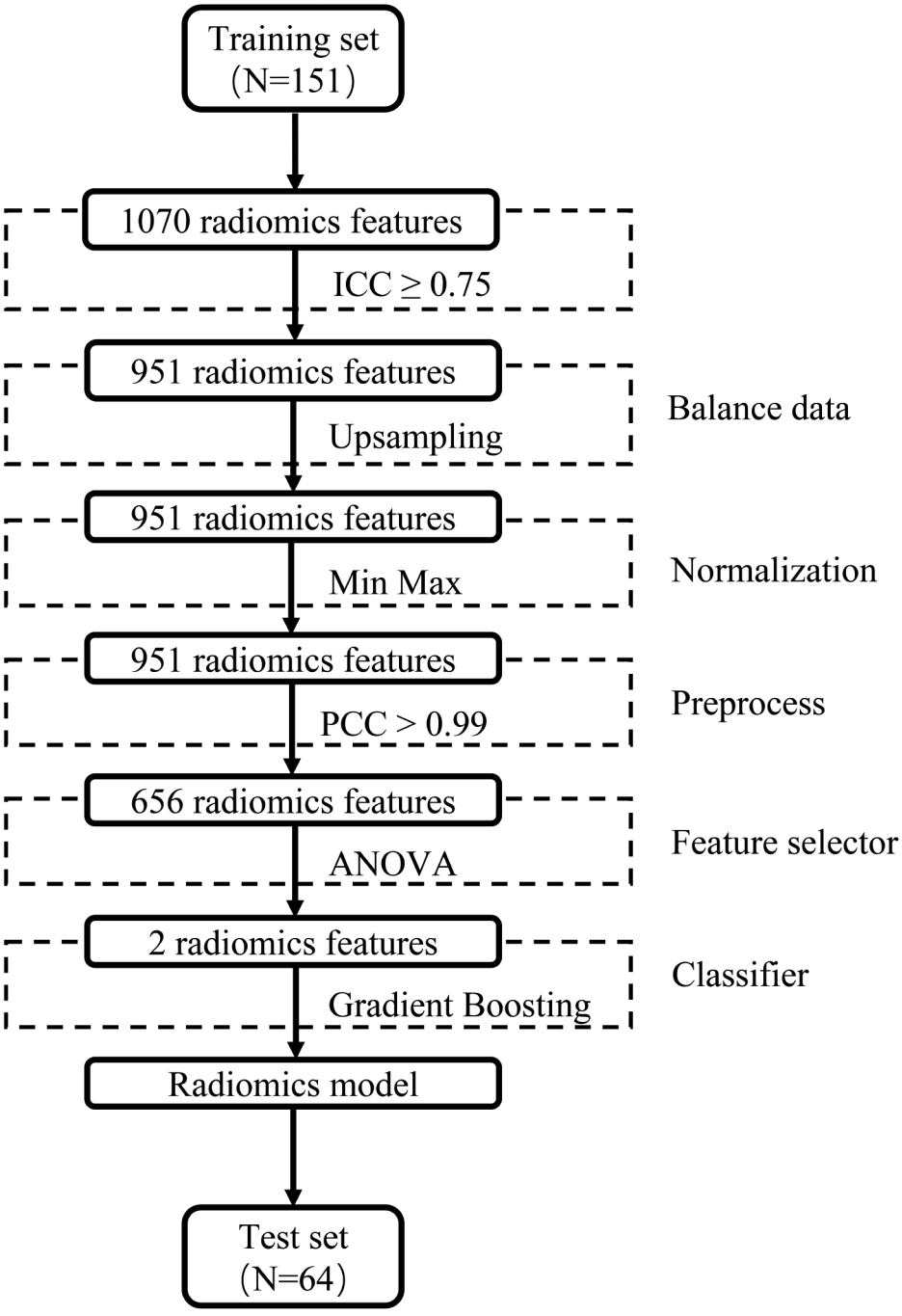

Fig. 3 The flowchart of the radiomics model construction. A total of 951 features were retained based on ICC ≥ 0.75. To address class imbalance, upsampling was applied to the training set, followed by min–max normalization for standardization. Feature reduction using the Pearson correlation coefficient (threshold 0.99) reduced the feature set to 656, which was further refined to 2 features using Analysis of Variance (ANOVA). Gradient boosting classifiers were then trained on these optimized features using the balanced training set

co-occurrence matrix (GLCM)-derived texture features. These two characteristics highlight the model's ability to capture both basic intensity distributions and complex textural patterns.

Our results confirm that the texture features of the GLCM are highly important for distinguishing between low- and high-grade UTUC. The texture feature of the GLCM assesses the textural characteristics of an image by analyzing the spatial alignment statistics of the pixel intensity, which is known to reflect the heterogeneity of tumors. For instance, GLCM has been used to distinguish low-grade bladder cancer from high-grade forms using DWI and ADC maps [28]. Additionally, the GLCM has been employed in the development and validation of a

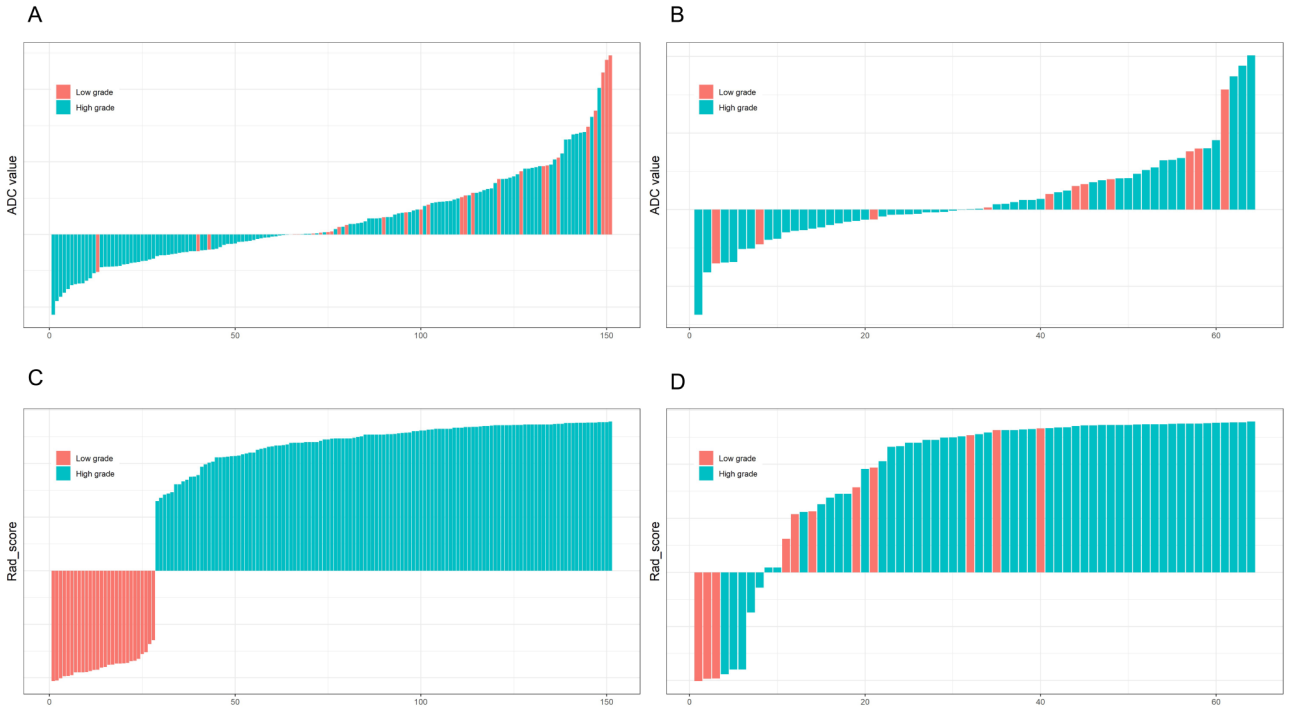

Fig. 4 Waterfall plots showing the distribution of ADC values and pathological grades (**A**, **B**) and radiomics scores and pathological grades (**C**, **D**) for individual patients in the training and test sets, respectively

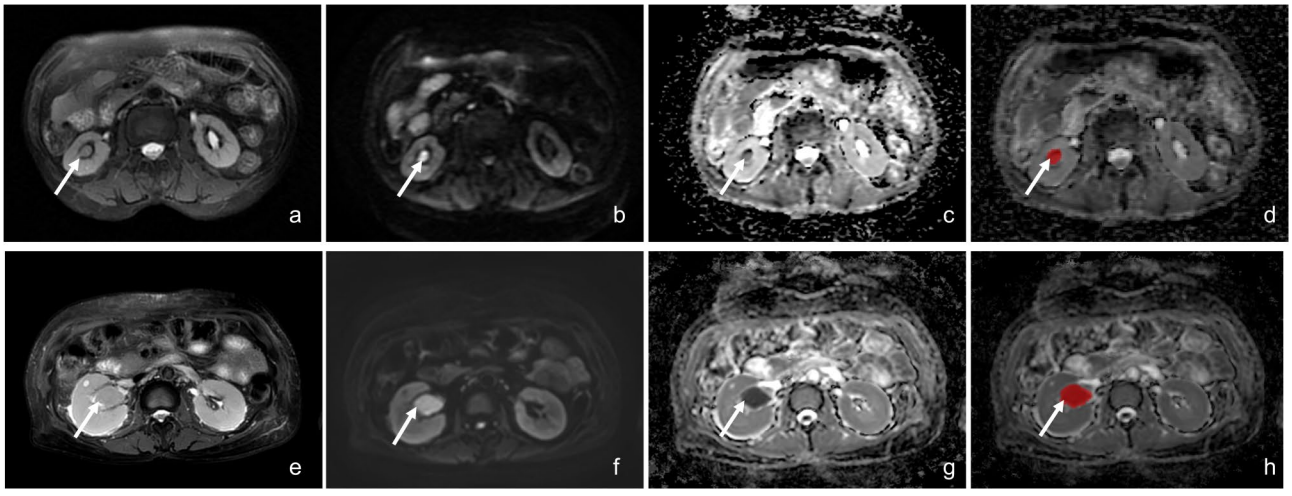

Fig. 5 Findings from two patients with histopathologically proven UTUC: low-grade (**a**–**d**) and high-grade (**e**–**h**). Images include axial T2WI (**a**, **e**), axial DWI (**b**, **f**; b = 1200 s/mm^2 and 800 s/mm^2, respectively), axial ADC maps (**c**, **g**), and VOIs manually annotated on the ADC maps (**d**, **h**). The long arrow indicates the lesion. Both lesions showed moderate hyperintensity on T2WI and hyperintensity on DWI. On the ADC maps, the low-grade lesion exhibited slight isointensity, while the high-grade lesion appeared hypointense. The mean ADC value of the low-grade UTUC was 1511×10^{-6} mm^2/s, with the radiomics model predicting high-grade UTUC for this case with a probability of 0.751. For the high-grade UTUC, the mean ADC value was 1283×10^{-6} mm^2/s, and the radiomics model correctly predicted high-grade UTUC with a probability of 0.979

computed tomography urography (CTU)-based machine learning (ML) model for predicting the preoperative pathological grade of UTUC [29]. Moreover, the ADC also plays a significant role in grading within radiomics and should not be neglected. Our results showed that the 10th percentile ADC values are useful for distinguishing between different grades, as they describe the distribution of voxel intensity within a defined image region. Previous studies have suggested that lower percentiles of ADC values perform better in diagnosing, classifying, and grading malignancies than do higher percentiles [11, 29, 30]. These findings emphasize the importance of

Table 4 Performance of the mean ADC value and radiomic model

Model	AUC (95% CI)	Sensitivity (95% CI)	Specificity (95% CI)	Accuracy (95% CI)	*P* Value
Training set					
Mean ADC value	0.698 (0.625, 0.772)	0.504 (0.416,0.592)	0.893 (0.778, 1.000)	0.576 (0.573,0.579)	
Radiomics model	1.000 (1.000, 1.000)	1.000 (1.000, 1.000)	1.000 (1.000, 1.000)	1.000 (1.000, 1.000)	< 0.001*
Test set					
Mean ADC value	0.628 (0.474,0.782)	0.528 (0.394,0.663)	0.727 (0.464,0.990)	0.562 (0.555,0.570)	
Radiomics model	0.786 (0.651, 0.921)	0.755 (0.639, 0.871)	0.727 (0.464, 0.990)	0.750 (0.744, 0.756)	0.071 *

*Note**Comparison of ROC curve performance between the mean ADC value and the radiomics model using the DeLong test. AUC, area under curve; CI, confidence interval. ADC, Apparent diffusion coefficient

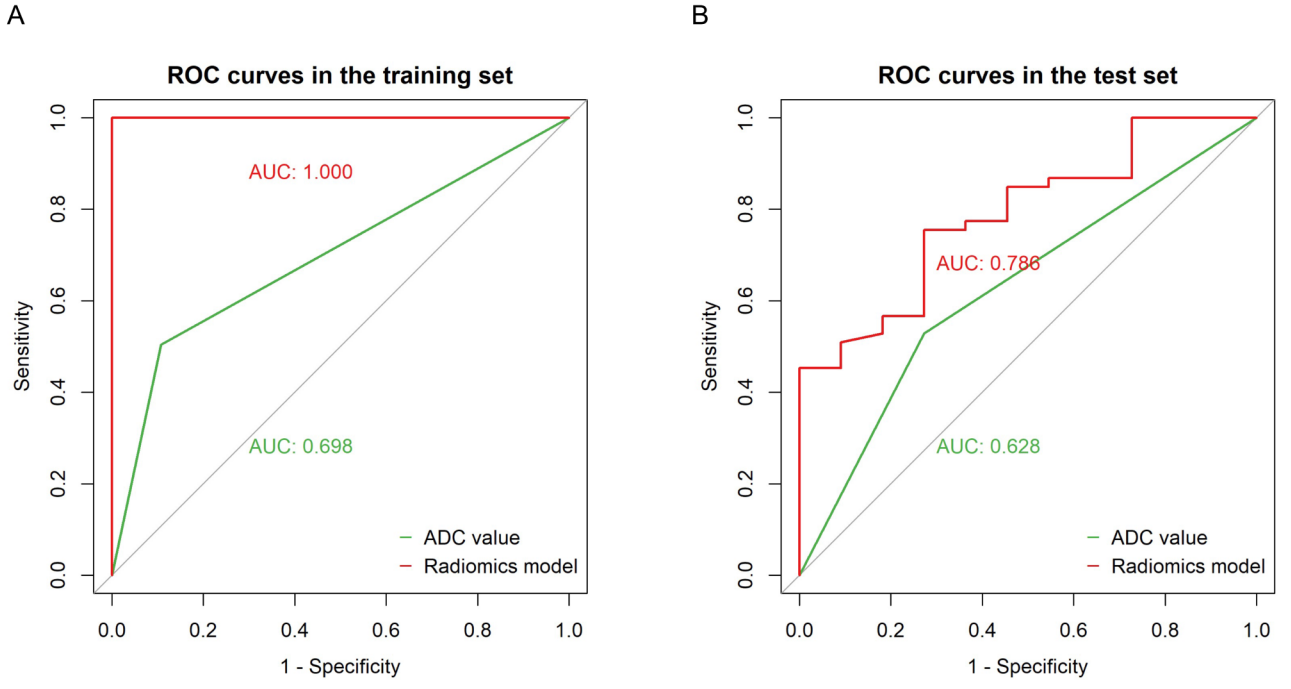

Fig. 6 ROC curves for the ADC value and radiomics model in the training (**A**) and test (**B**) sets

including both texture features and specific ADC values in radiomics analysis for a more accurate assessment of tumor grade.

We found that the AUC of the radiomics model was higher than that of the mean ADC in both the training set (1.000 vs. 0.698) and the test set (0.786 vs. 0.628), despite overlapping AUC confidence intervals in the test set. This suggests that ADC-based radiomics could be a more effective approach for preoperatively discriminating between different grades of UTUC. However, the difference in AUC between the radiomics model and the mean ADC values in the test set did not reach statistical significance, likely due to the relatively small sample size. To confirm these findings, future studies with larger cohorts and external validation are warranted. Additionally, we observed that the sensitivity of the radiomics model was consistently higher than that of the mean ADC values in both the training and test sets. This discrepancy may be influenced by various factors affecting ADC measurements. Beyond pathological factors, several imaging-related variables—such as field strength, respiratory compensation acquisition, b-value selection, and post-processing approaches—could significantly impact the accuracy and reliability of tumor ADC values [30]. In contrast, the radiomics model incorporates not only the ADC value but also texture features, which likely contribute to its superior sensitivity compared to the mean ADC value.

In the present study, we used ROC curve analyses and identified an ADC cutoff value of $1313\times10^{-6}mm^2/s$ as

the most useful for predicting the pathological grade of UTUC. An ADC<1313×10^{-6}mm^2/s predicted high-grade UTUC with a sensitivity of 50.4% and a specificity of 89.3%. Recently, Almås et al. [16] proposed a cutoff value of 1200×10^{-6}mm^2/s to distinguish the pathological grade of UTUC, with a sensitivity and specificity of 53% and 90%, respectively. Our cutoff value is notably higher than theirs, and several factors could account for this discrepancy. First, our study benefits from a substantially larger sample size, although the difference in the positive and negative sample data could affect the final results. Second, the diversity of our MR scanner setup, encompassing up to eight units with varying field strengths (1.5T/3.0T), contrasts with their singular reliance on a 3.0T MR scanner. This variability in imaging equipment could contribute to differences in ADC measurements. Finally, our methodology for determining the mean ADC, which utilizes automated three-dimensional VOI, offers a more comprehensive and potentially more accurate assessment than the manual two-dimensional region of interest (ROI) approach. These methodological differences underscore the potential for variability but also highlight the generalizability and applicability of our measurement techniques. The larger sample size, diverse imaging equipment, and advanced volumetric analysis in our study provide a robust framework for the use of ADC-based radiomics in grading UTUC, enhancing the accuracy and reliability of our findings. This comprehensive approach underscores the potential of our radiomics model to deliver more precise and reliable assessments of tumor grade, facilitating improved clinical decision-making.

There are several limitations to our study. Firstly, inherent bias may arise due to its retrospective nature, which could be addressed by employing a prospective study design in future research. Secondly, the study cohort, which was collected from a single institution, was neither large nor balanced enough, which may introduce bias in the decision boundary and limit the generalizability of the models. Although our study population was larger than that in most previous studies, the use of internal validation alone is a limitation, as it cannot fully account for variations in imaging protocols and patient populations across institutions. Therefore, external validation with multicenter datasets is essential to ensure the robustness and generalizability of the model in diverse clinical settings. Thirdly, our study included only ADC maps, which, while informative, provide limited insight into the full spectrum of tumor characteristics. Incorporating other imaging modalities, such as T2-weighted imaging and dynamic contrast-enhanced or perfusion-weighted images, could capture complementary features related to tumor morphology, vascularity, and microenvironment. These additional modalities may enhance the model's predictive performance and should be explored in future studies. Finally, various factors, such as image acquisition mode, reconstruction parameters, tumor segmentation method, and feature selection, could influence the results. Addressing these factors in future studies may further improve the robustness of ADC-based assessments.

In conclusion, the mean ADC values are helpful in discriminating between low- and high-grade UTUC. The ADC-based radiomics model showed promising potential in predicting the pathological grade of UTUC, outperforming the mean ADC values in classification accuracy. The ADC-based radiomics analysis presented herein offers promising advancements in the quantitative assessment of UTUC grades. Further studies with larger sample sizes and external validation are necessary to confirm its clinical utility and generalizability, highlighting the need for standardization in future studies.

Abbreviations

ADC	Apparent diffusion coefficient
ANOVA	Analysis of Variance
AUA	American Urology Association
AUC	Area under the curve
CI	Confidence interval
EAU	European Association of Urology
GLCM	Gray level co-occurrence matrix
ICC	Intraclass correlation coefficient
KSS	Kidney-sparing surgery
ML	Machine learning
RNU	Radical nephroureterectomy
ROC	Receiver operating characteristic
ROI	Region of interest
URS	Ureteroscopy
UTUC	Upper urinary tract urothelial carcinoma
VOI	Volumetric of interest

Supplementary Information

The online version contains supplementary material available at https://doi.org/10.1186/s12880-024-01540-w.

Supplementary Material 1

Acknowledgements
Not applicable.

Author contributions
Conceptualization: Rile Nai, Xiaoying Wang; Data curation: Rile Nai, Zuqiang Xi, Xiaoying Wang; Formal analysis: Rile Nai; Kexin Wang; Investigation: Rile Nai; Methodology: Rile Nai, Kexin Wang, Shuai Ma, Zuqiang Xi, Yaofeng Zhang, Xiaodong Zhang, Xiaoying Wang; Project administration: Xiaodong Zhang, Xiaoying Wang; Resources: Xiaodong Zhang, Xiaoying Wang; Software: Zuqiang Xi, Yaofeng Zhang; Supervision: Xiaoying Wang; Writing-original draft: Rile Nai; Writing-review & editing: Xiaoying Wang.

Funding
Not applicable.

Data availability
The datasets generated and/or analyzed in the current study are available from the corresponding author upon reasonable request.

Declarations

Ethics approval and consent to participate

This study was conducted in accordance with the declaration of Helsinki. This retrospective study was approved by the institutional ethics review board of Peking University First Hospital, which waived the requirement for informed consent (IRB number: 2023437).

Consent for publication

Not applicable.

Competing interests

The authors declare no competing interests.

Received: 7 October 2024 / Accepted: 18 December 2024
Published online: 30 December 2024

References

1. Siegel RL, Miller KD, Fuchs HE, Jemal A, Cancer statistics. 2022. CA: A Cancer Journal for Clinicians. 2022;72(1):7–33. https://doi.org/10.3322/caac.21708
2. Rouprêt M, Seisen T, Birtle AJ, et al. European Association of Urology Guidelines on Upper urinary tract Urothelial Carcinoma: 2023 update. Eur Urol. 2023;84(1):49–64. https://doi.org/10.1016/j.eururo.2023.03.013.
3. Mbeutcha A, Rouprêt M, Kamat AM, et al. Prognostic factors and predictive tools for upper tract urothelial carcinoma: a systematic review. World J Urol. 2017;35(3):337–53. https://doi.org/10.1007/s00345-016-1826-2.
4. Cutress ML, Stewart GD, Zakikhani P, Phipps S, Thomas BG, Tolley DA. Ureteroscopic and percutaneous management of upper tract urothelial carcinoma (UTUC): systematic review. BJU Int. 2012;110(5):614–28. https://doi.org/10.1111/j.1464-410X.2012.11068.x.
5. Smith AK, Stephenson AJ, Lane BR, et al. Inadequacy of biopsy for diagnosis of upper tract urothelial carcinoma: implications for conservative management. Urology. 2011;78(1):82–6. https://doi.org/10.1016/j.urology.2011.02.038.
6. Baard J, Cormio L, Dasgupta R, et al. Unveiling the challenges of UTUC biopsies and cytology: insights from a global real-world practice study. World J Urol. 2024;42(1):177. https://doi.org/10.1007/s00345-024-04866-w.
7. Ghoreifi A, Douglawi A, Djaladat H. The impact of Upper Tract Urothelial Carcinoma Diagnostic modality on Intravesical recurrence after Radical Nephroureterectomy: a single Institution Series and updated Meta-analysis. Letter J Urol. 2021;206(4):1071–1071. https://doi.org/10.1097/JU.0000000000001928.
8. Hoffmann E, Masthoff M, Kunz WG, et al. Multiparametric MRI for characterization of the tumour microenvironment. Nat Rev Clin Oncol. 2024;21(6):428–48. https://doi.org/10.1038/s41571-024-00891-1.
9. Kiessling F, Jugold M, Woenne EC, Brix G. Non-invasive assessment of vessel morphology and function in tumors by magnetic resonance imaging. Eur Radiol. 2007;17(8):2136–48. https://doi.org/10.1007/s00330-006-0566-x.
10. Lee SE, Jung JY, Nam Y, et al. Radiomics of diffusion-weighted MRI compared to conventional measurement of apparent diffusion-coefficient for differentiation between benign and malignant soft tissue tumors. Sci Rep. 2021;11(1):15276. https://doi.org/10.1038/s41598-021-94826-w.
11. Ren J, Yuan Y, Wu Y, Tao X. Differentiation of orbital lymphoma and idiopathic orbital inflammatory pseudotumor: combined diagnostic value of conventional MRI and histogram analysis of ADC maps. BMC Med Imaging. 2018;18(1):6. https://doi.org/10.1186/s12880-018-0246-8.
12. Park SY, Kim CK, Park BK, Kwon GY. Comparison of apparent diffusion coefficient calculation between two-point and multipoint B value analyses in prostate cancer and benign prostate tissue at 3 T: preliminary experience. AJR Am J Roentgenol. 2014;203(3):W287–294. https://doi.org/10.2214/AJR.13.11818.
13. Vallini V, Ortori S, Boraschi P, et al. Staging of pelvic lymph nodes in patients with prostate cancer: usefulness of multiple b value SE-EPI diffusion-weighted imaging on a 3.0 T MR system. Eur J Radiol Open. 2016;3:16–21. https://doi.org/10.1016/j.ejro.2015.11.004.
14. Akita H, Jinzaki M, Kikuchi E, et al. Preoperative T categorization and prediction of Histopathologic Grading of Urothelial Carcinoma in Renal Pelvis using diffusion-weighted MRI. Am J Roentgenol. 2011;197(5):1130–6. https://doi.org/10.2214/AJR.10.6299.
15. Yoshida S, Kobayashi S, Koga F, et al. Apparent diffusion coefficient as a prognostic biomarker of upper urinary tract cancer: a preliminary report. Eur Radiol. 2013;23(8):2206–14. https://doi.org/10.1007/s00330-013-2805-2.
16. Almås B, Reisæter LAR, Markhus CE, Hjelle KM, Børretzen A, Beisland C. A preoperative magnetic resonance imaging can aid in staging and treatment choice for upper tract urothelial carcinoma. BJUI Compass. 2024;5(5):476–82. https://doi.org/10.1002/bco2.337.
17. Lin WC, Chen JH. Pitfalls and limitations of Diffusion-Weighted Magnetic Resonance Imaging in the diagnosis of urinary bladder Cancer. Transl Oncol. 2015;8(3):217–30. https://doi.org/10.1016/j.tranon.2015.04.003.
18. Kocak B, Kus EA, Kilickesmez O. How to read and review papers on machine learning and artificial intelligence in radiology: a survival guide to key methodological concepts. Eur Radiol. 2021;31(4):1819–30. https://doi.org/10.1007/s00330-020-07324-4.
19. Li L, Zhang J, Zhe X, et al. An MRI-based radiomics nomogram in predicting histologic grade of non-muscle-invasive bladder cancer. Front Oncol. 2023;13. https://doi.org/10.3389/fonc.2023.1025972.
20. Coleman JA, Clark PE, Bixler BR, et al. Diagnosis and management of non-metastatic Upper Tract Urothelial Carcinoma: AUA/SUO Guideline. J Urol. 2023;209(6):1071–81. https://doi.org/10.1097/JU.0000000000003480.
21. Subiela JD, Territo A, Mercadé A, et al. Diagnostic accuracy of ureteroscopic biopsy in predicting stage and grade at final pathology in upper tract urothelial carcinoma: systematic review and meta-analysis. Eur J Surg Oncol. 2020;46(11):1989–97. https://doi.org/10.1016/j.ejso.2020.06.024.
22. Guo R, Hong P, Xiong G, et al. Impact of ureteroscopy before radical nephroureterectomy for upper tract urothelial carcinomas on oncological outcomes: a meta-analysis. BJU Int. 2018;121(2):184–93. https://doi.org/10.1111/bju.14053.
23. Yoshida S, Masuda H, Ishii C, et al. Usefulness of diffusion-weighted MRI in diagnosis of Upper urinary tract Cancer. Am J Roentgenol. 2011;196(1):110–6. https://doi.org/10.2214/AJR.10.4632.
24. Fan C, Sun K, Min X, et al. Discriminating malignant from benign testicular masses using machine-learning based radiomics signature of appearance diffusion coefficient maps: comparing with conventional mean and minimum ADC values. Eur J Radiol. 2022;148:110158. https://doi.org/10.1016/j.ejrad.2022.110158.
25. Donati OF, Mazaheri Y, Afaq A, et al. Prostate cancer aggressiveness: assessment with whole-lesion histogram analysis of the apparent diffusion coefficient. Radiology. 2014;271(1):143–52. https://doi.org/10.1148/radiol.13130973.
26. Zheng Y, Shi H, Fu S, et al. A computed tomography urography-based machine learning model for predicting preoperative pathological grade of upper urinary tract urothelial carcinoma. Cancer Med. 2024;13(1):e6901. https://doi.org/10.1002/cam4.6901.
27. Kierans AS, Doshi AM, Dunst D, Popiolek D, Blank SV, Rosenkrantz AB. Retrospective Assessment of Histogram-based Diffusion Metrics for differentiating Benign and malignant endometrial lesions. J Comput Assist Tomogr. 2016;40(5):723–9. https://doi.org/10.1097/RCT.0000000000000430.
28. Zhang X, Xu X, Tian Q, et al. Radiomics assessment of bladder cancer grade using texture features from diffusion-weighted imaging. J Magn Reson Imaging. 2017;46(5):1281–8. https://doi.org/10.1002/jmri.25669.
29. Dale BM, Braithwaite AC, Boll DT, Merkle EM. Field strength and diffusion encoding technique affect the apparent diffusion coefficient measurements in diffusion-weighted imaging of the abdomen. Invest Radiol. 2010;45(2):104–8. https://doi.org/10.1097/RLI.0b013e3181c8ceac.
30. Zhang L, Li X, Yang L, et al. Multi-sequence and Multi-regional MRI-Based Radiomics Nomogram for the Preoperative Assessment of muscle Invasion in bladder Cancer. J Magn Reson Imaging. 2023;58(1):258–69. https://doi.org/10.1002/jmri.28498.

Publisher's note